NiO/Graphene Composite for Enhanced Charge Separation and Collection in p–Type Dye Sensitized Solar Cell

8 AUTHORS, INCLUDING:

Hong Bin Yang
Nanyang Technological University
81 PUBLICATIONS   1,730 CITATIONS

SEE PROFILE

San Ping Jiang
Curtin University
344 PUBLICATIONS   11,150 CITATIONS

SEE PROFILE

Wang Yilei
10 PUBLICATIONS   118 CITATIONS

SEE PROFILE

Chang Li
Xin Xiang Medical University
390 PUBLICATIONS   12,632 CITATIONS

SEE PROFILE

NiO/Graphene Composite for Enhanced Charge Separation and Collection in p-Type Dye Sensitized Solar Cell

Hongbin Yang,[†] Guan Hong Guai,[†] Chunxian Guo,[†,‡] Qunliang Song,[‡] San Ping Jiang,[§] Yilei Wang,[†] Wei Zhang,[†] and Chang Ming Li*[,†,‡]

[†]School of Chemical and Biomedical & Center for Advanced Bionanosystems, Nanyang Technological University, 70 Nanyang Drive, Singapore 637457, Singapore

[‡]Institute for Clean Energy & Advanced Materials, Southwest University, Chongqing 400715, P. R. China

[§]Curtin Centre for Advanced Energy Science and Engineering, Department of Chemical Engineering, Curtin University of Technology, Perth, WA 6845, Australia

Ⓢ *Supporting Information*

ABSTRACT: A p-type semiconductor photoelectrode in dye sensitized solar cells (DSCs) has a large optical band gap and high ionization potential but suffers from its intrinsically low hole transfer rate, thus resulting in much poorer performance than n-DSCs. Nickel oxide (NiO)/graphene composite is synthesized to offer a larger surface area and higher conductivity than the pristine NiO film. The novel composite as a photoelectrode in p-DSCs demonstrates increment of both short-circuit photocurrent and open-circuit photovoltage, leading to 2 times increase of power conversion efficiency. Electrochemical impedance spectroscopy and open-circuit voltage decay measurements indicate that the charge recombination of the composite-based p-DSCs is significantly suppressed due to enhanced hole transport by the presence of graphene, thus achieving an efficient electron—hole pair charge separation and collection in the composite film electrode for performance-improved NiO-based devices. The proposed mechanism provides physical insight into the enhancement process in p-DSCs.
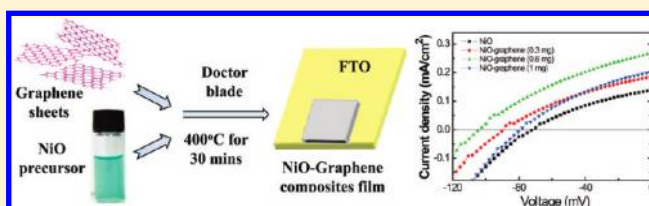
1. INTRODUCTION

Recently, a p-type semiconductor, nickel oxide (NiO), has been reported as a potential photocathode material for dye sensitized solar cells (DSCs) due to its large optical band gap (ca. 3.4 eV) and high ionization potential (5.4 eV vs vacuum) as a particularly good electron donor suitable to many photosensitizers.[1-3] With using a tandem structure constituting a TiO_2 photoanode and a NiO photocathode, the open-circuit voltage of the DSCs is increased.[4] Some p-type dyes[5,6] and electrolyte[4] have been also synthesized to further improve the performance of p-DSCs. However, its overall performance is still much lower than that of n-DSCs. One major limitation is the low intrinsic electric conductivity and hole diffusion coefficient of NiO film ($\sim 10^{-8}-10^{-7}$ cm^2 S^{-1}, more than 2 orders of magnitude lower than the electron diffusion coefficient of TiO_2),[3,4] resulting in loss of photogenerated hole through recombination with the excited state of electrolyte and the excited electron in dye molecule.[7] Therefore, it is necessary to suppress the back-reactions of p-DSCs by enhancing hole transport in NiO photocathode to effectively extract the photogenerated holes to the external circuit.[8] Graphene, a two-dimensional atomic sheet of carbon atom, has attracted much attention nowadays due to its unique properties, such as a large specific surface area, high electric conductivity, and high transparency[9-11] since its discovery by Geim.[12] Different nanomaterials such as gold nanoparticles,[13] metal oxide nanoparticles,[14-19] conducting polymer,[20,21] and quantum dots[22,23] have been immobilized on graphene or graphene oxide sheets to form

graphene-based hybrid nanomaterials for different applications such as transistors,[24] sensors,[18,25,26] hydrogen storage,[27,28] lithium ion batteries,[17-19] and solar cells applications.[21,29,30] In the field of dye sensitized solar cells (DSCs), graphene has been incorporated into the TiO_2 film by many approaches for high performance n-type DSCs.[31,32] It has been displayed that the graphene sheets can serve as a shuttle to enhance the electron transporting and suppress the recombination in n-type DSCs for performance enhancement. Introduction of graphene to NiO cathode may improve its charge transport.

In this work, NiO/graphene composite films were synthesized, characterized, and further used to fabricate photocathodes for performance improvement of p-DSCs. According to experimental results, the enhancement mechanism is proposed, and the fundamental physical insight is discussed.

2. EXPERIMENTAL SECTION

2.1. Synthesis of NiO/Graphene Composite. To synthesize the NiO/graphene composite, graphene sheets were first prepared by chemical exfoliation of flake graphite powder (Bay Carbon) followed by reduction as previously reported.[30] Nickel chloride

ACS Publications   © 2011 American Chemical Society

12209

dx.doi.org/10.1021/jp201178a | *J. Phys. Chem. C* 2011, 115, 12209–12215

Scheme 1. Synthesis Procedure for NiO/Graphene Composite Films

(NiCl$_2$) and triblock copolymer (F108) were purchased from Sigma and used as received. Scheme 1 illustrates the fabrication process of NiO/graphene composites films. Standard NiO precursor solution[33] was prepared by dissolving anhydrous NiCl$_2$ (1 g) and F108 (1 g) into a mixture of Mill-Q water (3 mL) and ethanol (6 mL). A measured amount of graphene (0.3, 0.6, and 1 mg) was then added into the standard NiO precursor solution and stirred to obtain a homogeneously dispersed NiO/graphene composite precursor. The synthesized composites were named according to the amount of graphene in the standard NiO precursor solution as NiO/graphene-0.3 mg, -0.6 mg, and -1.0 mg. (Figure S1 shows the digital pictures of various precursor solutions and 0.2 mg/mL graphene aqueous solution.) Subsequently, NiO/graphene composite films were prepared by applying the various precursor solutions onto patterned fluorine-doped tin oxide transparent substrates (FTO, 10 Ω/square) by doctor blade method and dried at room temperature, followed by an annealing at 400 °C for 30 min in air. The thickness of all the films was ~1 μm, and areas for all p-DSSCs test cells were 0.25 cm^{-2}. For comparison, NiO film was also prepared under the same conditions without the presence of graphene sheets.

2.2. Materials Characterizations. The graphene sheets were characterized by atomic force microscopy (AFM, Nanoman, Veeco, Santa Barbara, CA) using tapping mode. The NiO and NiO/graphene composites were investigated by field emission scanning electron microscopy (FE-SEM, JSM-6700F, Japan), transmission electron microscopy (TEM, JEOL 2010, Japan), and X-ray diffraction (D8 advance X-ray diffractometer, Bruker AXS, German, λ = 0.154 18 nm). The Brunauer—Emmett—Teller (BET) surface areas of NiO and NiO/graphene composites were measured with Autosorb-6B (Quantachrome Instruments). The NiO and NiO/graphene were scraped off from the films, identical to those used in the solar cells, and collected to measure the BET surface areas. UV—vis absorption and Raman spectra of the samples were measured using a spectrophotometer (UV-2450, Shimadzu) and a Renishaw 1000 microspectrometer (excitation wavelength of 514.5 nm), respectively.

2.3. Fabrication and Characterization of p-DSCs. The sensitizer dye (N719, (Bu$_4$N)$_2$[Ru(Hdcbpy)$_2$(NCS)$_2$], Solaronix SA) was dissolved for a concentration of 0.5 mM in a mixture of *tert*-butyl alcohol and acetonitrile (1:1 w/w). The as-prepared NiO and NiO/graphene composite films were immersed in the dye solution at room temperature for 16 h, followed by rinsing in ethanol and drying in air. The p-DSSCs were composed of the fabricated oxide photocathode, a platinum-coated ITO counter electrode, and electrolyte containing 0.8 M LiI and 0.15 M I$_2$ in acetonitrile. The current density (J)—voltage (V) characteristics were measured by a Keithley 2420 in dark and under illumination of a sun 2000 solar simulator (Abet) with 100 mW/cm^2 AM1.5G
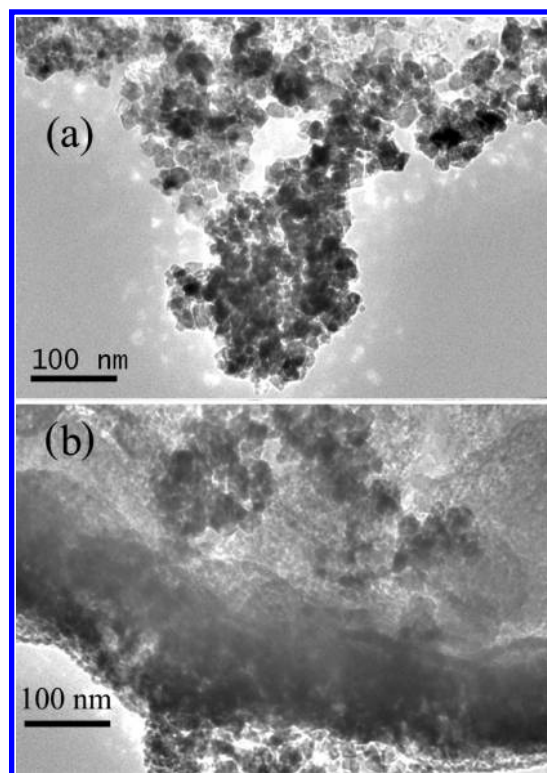
Figure 1. TEM micrograph of (a) NiO nanoparticles and (b) NiO/graphene composite.

spectrum. The intensity of the solar simulator was calibrated by a standard Si photovoltaic cell. Incident photon-to-electron conversion efficiency (IPCE) measurements were performed without bias illumination in respect to a calibrated silicon diode. The monochromic light was supplied by xenon light illuminating through a Cornerstone monochromator. A chopper was placed after the monochromator, and the signal was collected by Merlin lock-in radiometry after amplification by the current preamplifier. Electrochemical impedance spectroscopy (EIS) was performed with Solartron 1260 + 1294 impedance analyzer under illumination at open-circuit potential in a range from 100 000 to 0.1 Hz with ac amplitude of 15 mV.

3. RESULTS AND DISCUSSION

The structures of NiO and NiO/graphene composite were characterized by TEM and XRD. TEM images of NiO nanoparticles and NiO/graphene nanoparticle composite in Figure 1 show that the size of NiO particles is uniform distributed in the range of 15—20 nm (Figure 1a), which is in agreement with the mean crystal size value of 16 nm calculated by the Scherrer equation based on (200) peak from the X-ray diffraction spectra (see Figure S2). The graphene sheets and the spherical nanostructures of NiO particles can be observed in Figure 1b, signifying the successful incorporation of NiO nanoparticles onto graphene for a composite. The XRD patterns show that the NiO particles are single FCC phase in both plain NiO and NiO/graphene composite films. The result is in accordance with that of the standard spectrum (JCPDS, No. 04-0835), indicating the crystal structure of NiO is not affected by incorporation of graphene sheets.

The presence of graphene sheets in the composite is proven in the UV—vis spectra (Figure 2a), in which the absorption
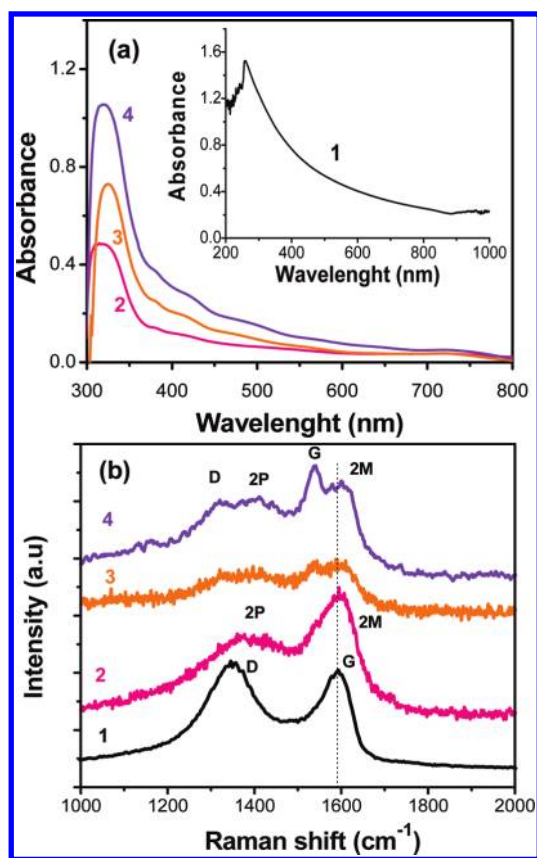
12210

dx.doi.org/10.1021/jp201178a |*J. Phys. Chem. C* 2011, 115, 12209–12215

Figure 2. (a) UV−vis and (b) Raman spectra of graphene (1), NiO (2), and NiO/graphene composite films with different graphene amounts, 0.3 mg (3) and 0.6 mg in 1 g of Nickel chloride (4).
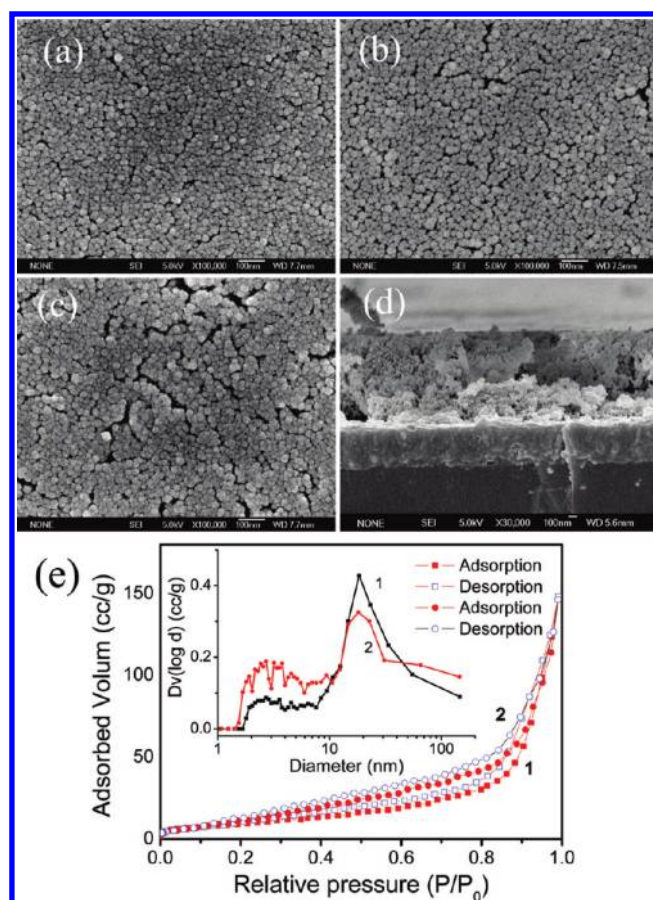

Figure 3. SEM images of (a) NiO and NiO/graphene composite films with different amount of graphene (b, 0.6 mg; c, 1.0 mg), (d) cross section of the composite, and (e) the nitrogen adsorption/desorption isotherms (1 for NiO, 2 for NiO/graphene-0.6 mg). Inset: BJH pore size distributions calculated from N_2 desorption isotherms.

intensity increases in the UV and visible regions with increasing graphene amount in the composite. The absorption peak located at around 320 nm was due to direct excitation of the NiO. The enhanced absorption can be attributed to the chemically reduced graphene as in accordance with the UV−vis spectrum of plain graphene (the inset of Figure 2a). Raman spectroscopy was employed to obtain the global structural information on the NiO/graphene composites, showing the D band (1349 cm^{-1}) and G band (1587 cm^{-1}) from the chemically reduced graphene, in which the former corresponds to the defect and the size of the in-plane sp^2 domain of graphene sheets.[34,35] The Raman spectrum of NiO nanoparticle (trace 2 in Figure 2b) displays two vibrational bands at 1392 and 1593 cm^{-1} that correspond to the two-magnon (2M) and two-phonon (2P) models.[36] Four peaks can be observed in the Raman spectra of NiO/graphene composites with different graphene loadings. The intensity of the peak around 1540 cm^{-1} increases considerably with higher graphene concentration in the composites, thus the matching peak to be the G band of graphene sheets. In comparison with graphene and NiO, significant shifts are observed in the vibrational bands of NiO/graphene composites. The D and G bands of graphene are blue-shifted from 1349 and 1587 cm^{-1} to 1314 and 1538 cm^{-1}, respectively. (Analysis of Raman spectrum of NiO/graphene composite is shown in Figure S4 and Table S1.) Moreover, the I_D/I_G intensity ratio of graphene is also reduced from 4.1 in graphene to 2.2 in NiO/graphene composite. For the NiO component, the 2M and 2P bands are shifted from 1392 and 1593 cm^{-1} to 1406 and 1608 cm^{-1}, respectively. The significant

vibrational band shifts of the graphene and NiO components in NiO/graphene composite indicate strong electrical interaction between NiO nanoparticles and graphene sheets, which would be favorable to charge transport from NiO nanoparticle into graphene sheets.

The FE-SEM images show the surface and cross-sectional morphologies of NiO and NiO/graphene composite films. At a low graphene amount, the NiO/graphene composite film has a higher porosity than that of plain NiO nanoparticle film. When the graphene amount is further increased to 1.0 mg, cracks start to appear due to aggregation of the graphene sheets in the precursor solution. From the cross-sectional image, the thickness of the NiO/graphene composite film is verified to be ∼1 μm. The increase in the porosity of NiO/graphene composite film is expected to lead to a higher surface area and provide more sites for dye adsorption. The surface areas and pore size distributions of the porous structure of NiO and NiO/graphene composite were obtained by the nitrogen adsorption/desorption isotherms as shown in Figure 3e. The BET surface area of NiO/graphene-0.6 mg composite is 66.1 m^2/g, ∼48% higher than that of plain NiO nanoparticle (44.8 m^2/g). Moreover, Barret−Joyner−Halenda (BJH) pore size distributions of NiO and NiO/graphene-0.6 mg composite show the NiO/graphene-0.6 mg composite has larger mesoporosity in the range of 2−10 nm. Because of the larger porosity and surface area of

NiO/graphene composite, more dye molecules can be effectively adsorbed onto the composite films. To determine the dye loading, the dye-loaded NiO and NiO/graphene photocathodes with an area of 2.2 cm^2 were desorbed using 4 mL of 0.1 M NaOH aqueous solution. The concentration of N719 dye solution was analyzed with a UV spectrometer at 535 nm. The N719 extinction coefficient at 535 nm is 1.47×10^4 L mol^{-1}. From the UV−vis spectra of the desorbed dye solutions (Figure S3), the amount of dye loading on NiO/graphene-0.6 mg composite electrode is 1.52×10^{-8} mol/cm^2, ~22.5% more than that of NiO electrode (1.24×10^{-8} mol/cm^2).

The $J−V$ characteristics and corresponding photovoltaic parameters of p-DSCs based on NiO and NiO/graphene composite films under 1 sun condition are depicted and summarized in Figure 4 and Table 1, respectively. The $J−V$ characteristics of devices in the dark show a diode behavior of the NiO/redox electrolyte interface (Figure 4a). Figure 4b shows that the devices performance related to the graphene concentration in the composites. When the graphene amount in the composite photocathode gradually increases to 0.6 mg, the J_{sc} and V_{oc} of p-DSCs increase and reach 0.27 mA/cm^2 and 105 mV, leading to
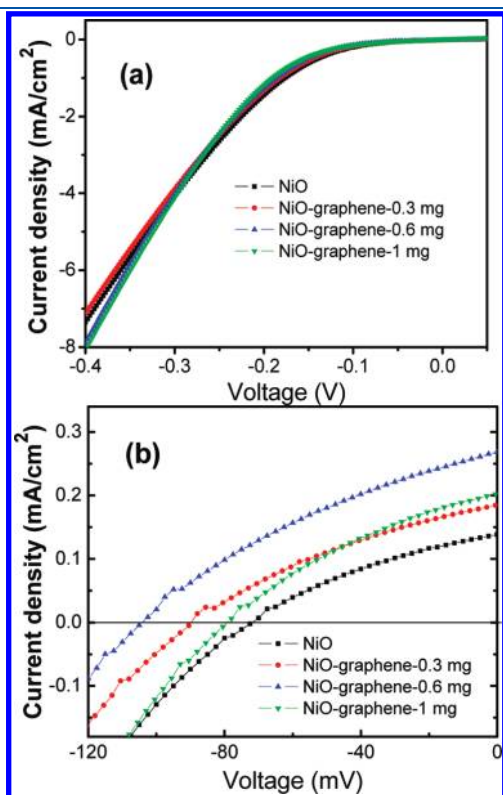

Figure 4. $J−V$ characteristics of p-DSSCs based on NiO and NiO/graphene composite films (a) in the dark and (b) under 1 sun intensity.

an efficiency of 0.0094%, which is almost 3 times that of p-DSSC with plain NiO as photocathode (0.0034%). As the graphene concentration further increases, the performance of the device starts to deteriorate. Figure 5 shows the IPCE and UV−vis absorption spectra for dye loaded NiO and NiO/graphene composite photocathodes. When the dye adsorbed on NiO, a blue-shift of maximum absorption from 538 to 520 nm against that measured in solution is observed (Figure S3), indicating a strong interaction between NiO and dye. Such a blue-shift has been observed for most the organic dyes absorbed on TiO$_2$ surface and can be partly attributed to the deprotonation of the carboxylic acid by adsorption on the NiO surface.[37−39] However, no obviously broaden absorption of dye loaded on NiO film is observed in comparison with that in solution, revealing that the dye loaded on NiO surface is a monomeric adsorption without aggregation. The IPCE spectra almost match with the dye absorption spectrum, suggesting that the photocurrent of p-DSCs is mainly generated by hole injection from the dye to NiO. The intensity of two peaks at ~320 and 400 nm shows slightly increase with increasing the graphene concentration in the composite films possibly due to the absorption of graphene. Nevertheless, it is an insignificant contribution to the enhancement of J_{sc}.

The influence of graphene concentration on the performance of p-DSCs can be explained based on effects of graphene on the hole transport of NiO/graphene composites. Scheme 2 represents the energy band diagram and proposed photogenerated hole transfer processes in the p-DSCs based on NiO/graphene composite photocathode. The ground state oxidation and reduction potentials of dye N719, NiO, and graphene in Scheme 2 are taken from refs 30 and 40. The difference of valence band of the NiO/composite from NiO is under investigations in our lab. Because of the difficulty, it will take times to draw conclusions for future report. After the light absorption and electron excitation, charge separation occurs at the NiO and dye interface by the hole injection into the NiO (T1) and the electron transfer from the excited state of dye to the electrolyte (T2). However, due to the low hole diffusion coefficient of NiO, some of the photogenerated holes tend to recombine with the excited electron (R1) and I$^−$/I$^{3−}$ ions (R2) prior effective extraction to the external circuit, resulting in a decrease of J_{sc}. Since the V_{oc} value of p-DSC is determined by the difference between the redox potential of I$^−$/I$^{3−}$ and Fermi level of NiO electrode, which in turn is directly related to the hole density in NiO electrode. Thus, the R1 and R2 processes also reduce the V_{oc} in p-DSCs. When NiO/graphene composite films are used as the photocathode, the injected holes can be transferred more rapidly from NiO nanoparticles (T3) into the graphene sheets, which serve as a shuttle to efficiently transport the holes to the external circuit, due to favorable energy level alignment and the strong interaction between NiO particle and graphene

Table 1. Photovoltaic Parameters for p-DSCs and Amount of Dye Loading with Different Electrodes Presented in Figure 4[a]

photocathode	V_{oc} (mV)	J_{sc} (mA/cm^2)	FF (%)	PCE (%)	amount of dye (10^{-8} mol/cm^2)
NiO	73	0.14	34	0.0034	1.24
NiO/graphene-0.3 mg	90	0.19	33	0.0056	1.31
NiO/graphene-0.6 mg	105	0.27	33	0.0094	1.52
NiO/graphene-1 mg	80	0.20	34	0.0054	1.19

[a] J_{sc}: short-circuit current density; V_{oc}: open-circuit current voltage; FF: fill factor; PCE: power conversion efficiency.

12212

dx.doi.org/10.1021/jp201178a |J. Phys. Chem. C 2011, 115, 12209−12215
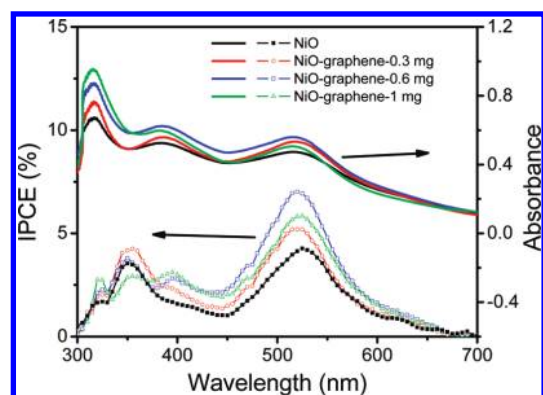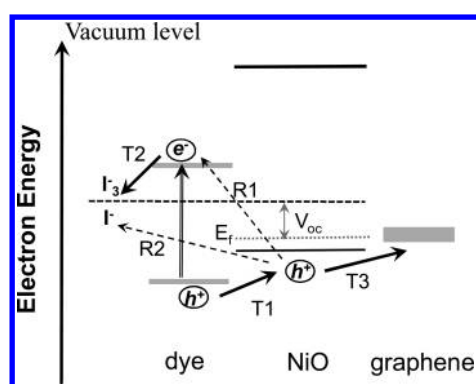
Figure 5. IPCE and UV−vis absorption spectra of NiO and NiO/graphene composite electrodes.

Scheme 2. Schematic Representation of Charge-Transfer Processes of p-DSCs[a]

[a] Solid and dashed arrows represent charge transport (desired) and recombination (undesired) processes, respectively.[3]
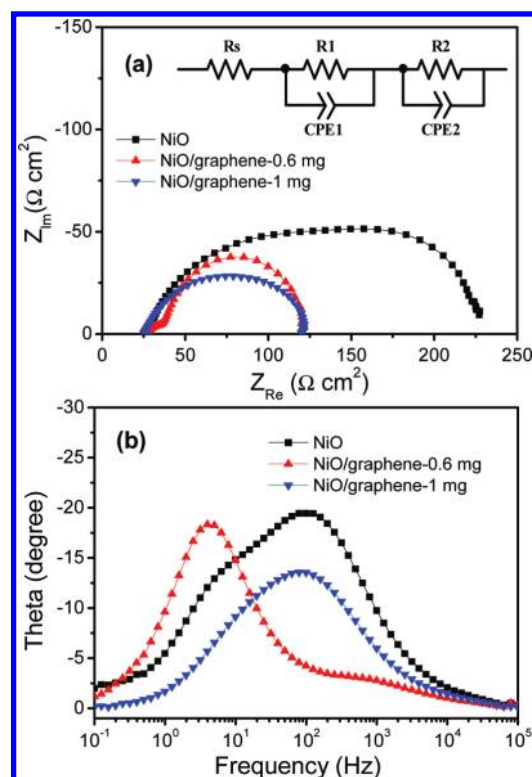

Figure 6. (a) Nyquist and (b) Bode diagrams of the EIS spectra of p-DSCs based on NiO and NiO/graphene composite electrodes. The spectra were measured under the illumination of 1 sun at open-circuit potential. Inset displays the equivalent circuit of the devices.

sheets, and results in significantly suppression of the R1 and R2 processes for enhancement of the p-DSCs performance.

In addition, for the composites films at low graphene amount (<0.6 mg), the dye loading increases with increase of the graphene concentration, achieving 1.52×10^{-8} mol/cm^2 for NiO/graphene-0.6 mg photocathode, which is higher than the plain NiO photocathode (1.24×10^{-8} mol/cm^2) by 22.5%. The higher dye loading leads to increased occurrences of photoexcitation events for more free charges to be generated in the photocathode. Thus, associated with the enhancement of hole transport by the graphene sheets, the J_{sc}, V_{oc}, and efficiency can be improved along with increasing the graphene concentration. For the NiO/graphene(1 mg) photocathode, the charge transport is further increased by more graphene sheets, but due to the lower dye loading (1.19×10^{-8} mol/cm^2) and the solar energy loss from the higher optical absorption of the NiO/graphene composite, much lesser free charges are generated, leading to a reduced J_{sc}. Furthermore, as shown in the FESEM images, large cracks in the composite film tend to result in the direct contact between the electrolyte and FTO electrode. Consequently, the recombination reaction between charges at FTO electrode with I^-/I_3^- in electrolyte would significantly reduce the J_{sc} and V_{oc} at a high graphene concentration. As discussed above, increasing the dye loading and enhancing the charge transport of

photocathode can significantly improve the p-DSCs performance. Thus, an intact, uniform, and thick mesoporous NiO/graphene film with high adsorption surface area will be a promising photocathode in p-DSCs although it is very difficult to be fabricated.

To further understand the role of graphene in the enhancement of hole transport in p-DSCs, EIS was performed at an applied bias of V_{oc} with ac amplitude of 15 mV under light illumination. Similar with EIS of n-DSCs, from Figure 6a, the semicircle at medium frequencies (ca. 1−100 Hz) of the Nyquist plots can be assigned to the hole transport in the mesoscopic NiO film and the back-reaction at the NiO/dye/electrolyte interface. The semicircles for the NiO/graphene composite electrodes are smaller than that for the plain NiO electrode, indicating a lower charge transfer impedance and faster hole transfer at the NiO/dye/electrolyte interface. Quantitative analysis of EIS was conducted based on a reported equivalent circuit,[41−43] where Rs, R1, and R2 represent the ohmic serial resistances for electrolyte/conductive glass, the platinum electrode, and NiO/dye/electrolyte interface, respectively. Compared with plain NiO photocathode, the NiO/graphene photocathodes have smaller R2 (14.5 and 22.1 Ω for graphene concentration at 0.6 and 1.0 mg, respectively, versus 118.4 Ω for plain NiO), thus clearly indicating an enhancement of the charge transfer in NiO/graphene photocathodes. The capacitance CPE2 at the NiO/dye/electrolyte interface also increases from 101 μF for plain NiO to 512 and 152 μF for NiO/graphene composites at 0.6 and 1.0 mg graphene concentration, respectively. The higher capacitance corresponds to the presence of more charges being separated effectively at the interface, thus indicating the reduction of charge recombination events in NiO/graphene

12213

dx.doi.org/10.1021/jp201178a |*J. Phys. Chem. C* 2011, 115, 12209−12215

composites. These results are also in agreement with the Bode plots illustrated in Figure 6b, in which the frequency peak position (f_{max}) related to the charge transfer at NiO/dye/electrolyte interface is shifted from 8 Hz for plain NiO electrode to a lower 4.5 Hz for NiO−graphene electrode. Since the charge carrier lifetime is inversely proportional to f_{max} a longer hole lifetime is present in the latter electrode. The hole lifetime (τ_n) estimated from the expression $\tau_n = 1/2\pi f_{max}$ (f_{max} is the peak frequency)[44] is 20 and 38 ms for NiO and NiO/graphene-0.6 mg electrode, respectively. The low hole transport resistance and long hole lifetime lead to reduction of recombination and capture of more effective hole. Open-circuit voltage decay (OCVD) measurements[45] performed further confirm the obtained conclusion from aforementioned EIS analysis (see Figure S4).

4. CONCLUSIONS

NiO/graphene composite films were synthesized, characterized, and further used to fabricate the photocathode for p-DSCs. The NiO/graphene composite with an appropriate graphene amount offers faster hole transport and larger surface area than that of the plain NiO film, thus leading to significant improvement of charge transfer and increase of dye loading, in turn resulting in the increase in both short-circuit photocurrent and open-circuit photovoltage. Both EIS and OCVD results show that the exciton effective separation and charge collection can be improved by using NiO/graphene composite films. An intact, uniform and thick mesoporous NiO/graphene film with high hole transport and large surface area will be a promising photocathode in p-DSCs although it is very difficult to be fabricated. The proposed mechanism provides the physics insight for the enhancement process in p-DSCs.

■ ASSOCIATED CONTENT

ⓢ Supporting Information. Digital pictures of graphene, $Ni(OH)_2$, and $Ni(OH)_2$/graphene mixture solution, X-ray diffraction spectra of the NiO and NiO/graphene composites with different graphene concentrations, UV−vis spectra of solutions containing N719 dye detached from NiO and NiO/graphene photocathodes, Raman spectra of NiO/graphene composite films, and open-circuit voltage decay profiles of NiO and NiO/ graphene composite photocathodes. This material is available free of charge via the Internet at http://pubs.acs.org.

■ AUTHOR INFORMATION

Corresponding Author
*Fax: +65 6791 1761; Tel: +65 6790 4485; e-mail: Ecmli@ ntu.edu.sg.

■ ACKNOWLEDGMENT

■ REFERENCES

(1) Morandeira, A.; Boschloo, G.; Hagfeldt, A.; Hammarström, L. *J. Phys. Chem. B* **2005**, *109*, 19403.

(2) Odobel, F.; Le Pleux, L. c.; Pellegrin, Y.; Blart, E. *Acc. Chem. Res.* **2010**, *43*, 1063.

(3) Mori, S.; Fukuda, S.; Sumikura, S.; Takeda, Y.; Tamaki, Y.; Suzuki, E.; Abe, T. *J. Phys. Chem. C* **2008**, *112*, 16134.

(4) Gibson, E. A.; Smeigh, A. L.; Le Pleux, L.; Fortage, J.; Boschloo, G.; Blart, E.; Pellegrin, Y.; Odobel, F.; Hagfeldt, A.; Hammarström, L. *Angew. Chem., Int. Ed.* **2009**, *48*, 4402.

(5) Qin, P.; Linder, M.; Brinck, T.; Boschloo, G.; Hagfeldt, A.; Sun, L. *Adv. Mater.* **2009**, *21*, 2993.

(6) Qin, P.; Wiberg, J.; Gibson, E. A.; Linder, M.; Li, L.; Brinck, T.; Hagfeldt, A.; Albinsson, B.; Sun, L. *J. Phys. Chem. C* **2010**, *114*, 4738.

(7) Uehara, S.; Sumikura, S.; Suzuki, E.; Mori, S. *Energy Environ. Sci.* **2010**, *3*, 641.

(8) Yang, H.; Song, Q.; Lu, Z.; Guo, C.; Gong, C.; Hu, W.; Li, C. M. *Energy Environ. Sci.* **2010**, *3*, 1580.

(9) Becerril, H. A.; Mao, J.; Liu, Z.; Stoltenberg, R. M.; Bao, Z.; Chen, Y. *ACS Nano* **2008**, *2*, 463.

(10) Li, X.; Zhu, Y.; Cai, W.; Borysiak, M.; Han, B.; Chen, D.; Piner, R. D.; Colombo, L.; Ruoff, R. S. *Nano Lett.* **2009**, *9*, 4359.

(11) Geim, A. K.; Novoselov, K. S. *Nature Mater.* **2007**, *6*, 183.

(12) Novoselov, K. S.; Geim, A. K.; Morozov, S. V.; Jiang, D.; Zhang, Y.; Dubonos, S. V.; Grigorieva, I. V.; Firsov, A. A. *Science* **2004**, *306*, 666.

(13) Muszynski, R.; Seger, B.; Kamat, P. V. *J. Phys. Chem. C* **2008**, *112*, 5263.

(14) Ng, Y. H.; Iwase, A.; Kudo, A.; Amal, R. *J. Phys. Chem. Lett.* **2010**, *1*, 2607.

(15) Williams, G.; Seger, B.; Kamat, P. V. *ACS Nano* **2008**, *2*, 1487.

(16) Ng, Y. H.; Lightcap, I. V.; Goodwin, K.; Matsumura, M.; Kamat, P. V. *J. Phys. Chem. Lett.* **2010**, *1*, 2222.

(17) Wang, H.; Cui, L.-F.; Yang, Y.; Sanchez Casalongue, H.; Robinson, J. T.; Liang, Y.; Cui, Y.; Dai, H. *J. Am. Chem. Soc.* **2010**, *132*, 13978.

(18) Guo, C. X.; Zheng, X. T.; Lu, Z. S.; Lou, X. W.; Li, C. M. *Adv. Mater.* **2010**, *22*, 5164.

(19) Meng, X.; Geng, D.; Liu, J.; Banis, M. N.; Zhang, Y.; Li, R.; Sun, X. *J. Phys. Chem. C* **2010**, *114*, 18330.

(20) Zhou, X.; Wu, T.; Hu, B.; Yang, G.; Han, B. *Chem. Commun.* **2010**, *46*, 3663.

(21) Yu, D.; Yang, Y.; Durstock, M.; Baek, J.-B.; Dai, L. *ACS Nano* **2010**, *4*, 5633.

(22) Lu, Z. S.; Guo, C. X.; Yang, H. B.; Qiao, Y.; Guo, J.; Li, C. M. *J. Colloid Interface Sci.* **2011**, *353*, 588.

(23) Zedan, A. F.; Sappal, S.; Moussa, S.; El-Shall, M. S. *J. Phys. Chem. C* **2010**, *114*, 19920.

(24) Cheng, Z.; Li, Q.; Li, Z.; Zhou, Q.; Fang, Y. *Nano Lett.* **2010**, *10*, 1864.

(25) Schedin, F.; Geim, A. K.; Morozov, S. V.; Hill, E. W.; Blake, P.; Katsnelson, M. I.; Novoselov, K. S. *Nature Mater.* **2007**, *6*, 652.

(26) Guo, C. X.; Lu, Z. S.; Lei, Y.; Li, C. M. *Electrochem. Commun.* **2010**, *12*, 1237.

(27) Wang, Y.; Guo, C. X.; Wang, X.; Guan, C.; Yang, H. B.; Wang, K.; Li, C. M. *Energy Environ. Sci.* **2011**, *4*, 195.

(28) Lee, H.; Ihm, J.; Cohen, M. L.; Louie, S. G. *Nano Lett.* **2010**, *10*, 793.

(29) Yang, H. B.; Guo, C. X.; Guai, G. H.; Song, Q. L.; Jiang, S. P.; Li, C. M. *ACS Appl. Mater. Interfaces* **2011** 10.1021/am200154h.

(30) Guo, C. X.; Yang, H. B.; Lu, Z. S.; Song, Q. L.; Sheng, Z. M.; Li, C. M. *Angew. Chem., Int. Ed.* **2010**, *49*, 3014.

(31) Tang, Y.-B.; Lee, C.-S.; Xu, J.; Liu, Z.-T.; Chen, Z.-H.; He, Z.; Cao, Y.-L.; Yuan, G.; Song, H.; Chen, L.; Luo, L.; Cheng, H.-M.; Zhang, W.-J.; Bello, I.; Lee, S.-T. *ACS Nano* **2010**, *4*, 3482.

(32) Yang, N.; Zhai, J.; Wang, D.; Chen, Y.; Jiang, L. *ACS Nano* **2010**, *4*, 887.

(33) Sumikura, S.; Mori, S.; Shimizu, S.; Usami, H.; Suzuki, E. *J. Photochem. Photobiol., A* **2008**, *199*, 1.

(34) Kudin, K. N.; Ozbas, B.; Schniepp, H. C.; Prud'homme, R. K.; Aksay, I. A.; Car, R. *Nano Lett.* **2007**, *8*, 36.

(35) Stankovich, S.; Dikin, D. A.; Piner, R. D.; Kohlhaas, K. A.; Kleinhammes, A.; Jia, Y.; Wu, Y.; Nguyen, S. T.; Ruoff, R. S. *Carbon* **2007**, *45*, 1558.

12214

dx.doi.org/10.1021/jp201178a |*J. Phys. Chem. C* 2011, 115, 12209–12215

(36) Dietz, R. E.; Brinkman, W. F.; Meixner, A. E.; Guggenheim, H. J. *Phys. Rev. Lett.* **1971**, *27*, 814.

(37) Hagberg, D. P.; Edvinsson, T.; Marinado, T.; Boschloo, G.; Hagfeldt, A.; Sun, L. *Chem. Commun.* **2006**, *21*, 2245.

(38) Qin, P.; Yang, X.; Chen, R.; Sun, L.; Marinado, T.; Edvinsson, T.; Boschloo, G.; Hagfeldt, A. *J. Phys. Chem. C* **2007**, *111*, 1853.

(39) Yen, Y.-S.; Hsu, Y.-C.; Lin, J. T.; Chang, C.-W.; Hsu, C.-P.; Yin, D.-J. *J. Phys. Chem. C* **2008**, *112*, 12557.

(40) Liu, Z.; Liu, Q.; Huang, Y.; Ma, Y.; Yin, S.; Zhang, X.; Sun, W.; Chen, Y. *Adv. Mater.* **2008**, *20*, 3924.

(41) van de Lagemaat, J.; Park, N. G.; Frank, A. J. *J. Phys. Chem. B* **2000**, *104*, 2044.

(42) Wang, Q.; Moser, J.-E.; Grätzel, M. *J. Phys. Chem. B* **2005**, *109*, 14945.

(43) Adachi, M.; Sakamoto, M.; Jiu, J.; Ogata, Y.; Isoda, S. *J. Phys. Chem. B* **2006**, *110*, 13872.

(44) Kern, R.; Sastrawan, R.; Ferber, J.; Stangl, R.; Luther, J. *Electrochim. Acta* **2002**, *47*, 4213.

(45) Bisquert, J.; Zaban, A.; Greenshtein, M.; Mora-Seró, I. *J. Am. Chem. Soc.* **2004**, *126*, 13550.